Research Paper
Computational Methods for Differential Equations
http://cmde.tabrizu.ac.ir
Vol. *, No. *, *, pp. 1-11
DOI:10.22034/cmde.2025.68151.3287

Application of stochastic Runge-Kutta methods for mixed fractional Brownian motion processes

Nader Karimi[1,*] **and Masoumeh Shahmoradi**[2]

[1]Department of Applied Mathematics, Faculty of Mathematics and Computer Sciences, Amirkabir University of Technology (Tehran Polytechnic), No. 424, Hafez Ave., 15914 Tehran, Iran.

[2]Department of Mathematics, Azarbaijan Shahid Madani University, Tabriz, Iran.

Abstract

We develop and analyze a stochastic Runge-Kutta (SRK) method for pricing derivatives when the underlying asset follows a mixed fractional Brownian motion (fBm). From this non-Markovian process we re-derive a Black-Scholes-type partial differential equation (PDE) and show that the proposed SRK integrator is both mean-square stable and strongly convergent. Sharp bounds for the stability region and the order of convergence are rigorously proved. Numerical experiments confirm the theory and demonstrate superior accuracy of the SRK method compared with Euler-Maruyama and Milstein schemes.

Keywords. Stochastic Runge-Kutta (SRK),Black-Scholes model; Euler-Maruyama and Milstein schemes, mixed Fractional Brownian motion(mFBm).

2010 Mathematics Subject Classification. 65L05, 34K06, 34K28.

1. Introduction

Classical Black–Scholes modeling assumes that the discounted asset price follows a geometric Brownian motion (GBM) with constant drift and volatility. This modeling choice implies Gaussian, memoryless log-returns and neglects empirically observed features such as long-range dependence, volatility clustering, and heavy tails [8, 13]. To address these limitations while preserving tractability, one widely adopted approach replaces the standard Brownian motion W_t with a fractional Brownian motion (fBm) B_t^H of Hurst index $H \in (0,1)$, introduced by Mandelbrot and Van Ness [13]. Unlike standard Brownian motion, fBm exhibits persistent ($H > 1/2$) or anti-persistent ($H < 1/2$) increments, better capturing the memory structure observed in high-frequency financial data [6, 15].

Despite its modeling appeal, fBm is not a semimartingale when $H \neq \frac{1}{2}$, making classical Itô calculus and arbitrage-free pricing tools inapplicable. To circumvent this issue, mixed fractional models have been introduced, typically of the form

$$\widetilde{W}_t = \beta W_t + (1-\beta)B_t^H, \quad \beta \in (0,1),$$

where W_t retains the semimartingale property needed for martingale pricing theory, while B_t^H introduces long-range dependence [7, 12]. These models offer more flexibility in capturing the volatility smile and term structure of implied volatility than standard GBM [10, 21].

From a numerical standpoint, solving stochastic differential equations (SDEs) under such mixed or purely fractional dynamics poses significant challenges. The rougher trajectories of fBm necessitate the design of specialized integration schemes. While theoretical foundations of such schemes are covered in monographs such as [5, 9], high-order numerical methods that remain efficient and stable under mixed-noise settings are still under development.

Recent works have made substantial progress in this direction. In particular, Ahmadian and collaborators have studied stability and convergence properties of several numerical schemes including stochastic Runge-Kutta, theta-Milstein, and split-step methods for SDEs and delay SDEs, some with jumps and memory effects [3, 16, 18]. They

Received: 14 July 2025 ; Accepted: 19 October 2025.
∗ Corresponding author. Email: nkarimi@aut.ac.ir.

have provided rigorous mean-square and exponential stability criteria for both standard and non-standard stochastic models, and proposed methods with enhanced convergence orders and computational efficiency [1, 2, 17].

Motivated by the lack of high-order schemes for fractional and mixed SDEs with jumps, this paper makes the following key contributions:

- We formulate a mixed fractional Black–Scholes model under an equivalent martingale measure (EMM), derive the associated fractional Fokker–Planck–Kolmogorov equation, and discuss the no-arbitrage condition under this hybrid noise structure.
- We develop a second-order stochastic Runge–Kutta (SRK) integrator that respects both the semimartingale and memory components of the driving noise. Mean-square stability and convergence of the method are rigorously established, extending the techniques of Neuenkirch and Nourdin [12] to mixed-noise frameworks.
- Comprehensive numerical experiments including Monte Carlo simulations and benchmark comparisons demonstrate that the proposed SRK scheme significantly outperforms classical Euler–Maruyama and Milstein methods in accuracy while maintaining comparable computational costs.

Our results build upon and unify recent advances in both theoretical stochastic numerics and financial modeling, offering a robust framework for simulating and analyzing complex systems driven by both memory and jump features.

The rest of the article is organised as follows. Section 2 recalls basic properties of fractional Brownian motion (fBm) and rough integrals, providing the mathematical foundation necessary for understanding mixed fractional Brownian motion (mFBM). Section 3 introduces the mixed-fractional pricing model, derives the corresponding stochastic differential equation (SDE), and establishes the existence and uniqueness of strong solutions. Section 4 develops the Stochastic Runge-Kutta (SRK) integrator, presents the main convergence theorem, and proves its stability and convergence properties. Section 5 reports numerical results, comparing the accuracy and efficiency of the SRK method with other established methods like Euler-Maruyama and Milstein. Finally, section 6 concludes the paper by summarizing the main findings and suggesting future directions.

2. Fractional Brownian Motion and Rough Integrals

This section summarises the analytic ingredients needed for the mixed-fractional pricing model and for the SRK discretisation analysed later. We first recall the main facts about fractional Brownian motion (fBm) and then outline three integration frameworks:Young, Skorokhod and rough paths, highlighting when each is available.

2.1. Fractional Brownian Motion.

Definition 2.1 (Fractional Brownian Motion)**.** Let $H \in (0,1)$ be a fixed *Hurst index*. A centred Gaussian process $B^H = \{B_t^H\}_{t\geq 0}$ on a probability space $(\Omega, \mathcal{F}, \mathbb{P})$ is called a *fractional Brownian motion* (fBm) with Hurst index H if its covariance function is

$$\mathbb{E}\big[B_t^H\, B_s^H\big] \;=\; \tfrac{1}{2}\big(t^{2H} + s^{2H} - |t-s|^{2H}\big), \qquad s,t \geq 0. \tag{2.1}$$

Key properties.

(1) **Self-similarity:** $B_{ct}^H \overset{d}{=} c^H B_t^H$.
(2) **Stationary increments:** $B_t^H - B_s^H$ depends only on $t-s$.
(3) **Long-range dependence:** $\mathrm{Cov}(B_{t+u}^H - B_u^H, B_{s+u}^H - B_u^H) \sim H(2H-1)\, t^{2H-2} s$ as $s \to \infty$ if $H > 1/2$.
(4) **p-variation & Hölder regularity:** paths are α-Hölder for every $\alpha < H$ but for no $\alpha \geq H$ (Kolmogorov continuity theorem).

For $H = \frac{1}{2}$ the process reduces to classical Brownian motion B.

2.2. Pathwise Young Integration.

Let $(X_t)_{t\in[0,T]}$ and $(Y_t)_{t\in[0,T]}$ be functions with Hölder exponents α and β, respectively.

Theorem 2.2 ([20]). *If $\alpha+\beta>1$ the Riemann sums $\sum_{[u,v]\in\pi} X_u\big(Y_v-Y_u\big)$ converge uniformly over all tagged partitions π as $|\pi|\to 0$; their limit defines the* Young integral $\int_0^T X_s\,dY_s$ *and satisfies*

$$\Big|\int_s^t X_r\,dY_r - X_s\big(Y_t-Y_s\big)\Big| \;\le\; C_{\alpha,\beta}\|X\|_{\alpha,[s,t]}\|Y\|_{\beta,[s,t]}\,(t-s)^{\alpha+\beta},$$

where $\|X\|_{\alpha,[s,t]}$ is the Hölder seminorm.

Implication for fBm. Because B^H is γ-Hölder for any $\gamma<H$, the Young integral $\int X\,dB^H$ exists whenever $H>1/2$ and X is α-Hölder with $\alpha+H>1$.

2.3. **Skorokhod / Malliavin Integration.** For $H<\frac12$ the Young condition fails. One can instead use Malliavin calculus, interpreting the integral as a divergence (Skorokhod) operator [9]. Given a square–integrable process $u=\{u_t\}_{t\in[0,T]}$ in the Sobolev space $\mathbb{D}^{1,2}$, define

$$\int_0^T u_t\,\delta B_t^H \;:=\; \delta(u),$$

where δ is the adjoint of the Malliavin derivative. When u is adapted and satisfies suitable integrability conditions, the Skorokhod integral coincides with the Itô integral (for $H=\frac12$) and enjoys an Itô–Isometry–type bound.

2.4. **Rough-Path Lift of fBm.** The rough-path framework yields a unified integration theory for all $H\in(0,1)$.

Theorem 2.3 (fBm admits a geometric rough path). *For every $H>0$ there exists a canonical enhancement $\mathbf{B}^H=(B^H,\mathbb{B}^H)$, where the second level*

$$\mathbb{B}^H_{s,t} \;=\; \int_{s<r_1<r_2<t} dB^H_{r_1}\otimes dB^H_{r_2}, \qquad 0\le s<t\le T,$$

makes $\mathbf{B}^H$ a geometric p-rough path for any $p>1/H$.

Idea of proof. For $H>\frac12$ second level exists as Young iterated integral. For $H<\frac12$ one defines $\mathbb{B}^H$ via Wiener chaos expansion and shows convergence in L^2 (cf. [11]). □

With this lift the rough integral $\int_0^T f(X_r)\,dB^H_r$ is well-defined for any controlled process X and $f\in C_b^3$, irrespective of H.

3. Mixed Fractional Brownian Motion and Asset Dynamics

In recent years the mixed fractional Brownian motion

$$X_t \;=\; B_t \;+\; \beta\,B_t^H, \qquad 0<H<1,\;\; \beta\in\mathbb{R},$$

has become an attractive candidate for modelling asset–price dynamics because (i) the Brownian component B_t retains short-term volatility and the martingale property, (ii) the fractional component B_t^H with Hurst index H captures long-range dependence and volatility clustering.

Definition and Properties. The covariance of mFBM with weight β is

$$\mathrm{Cov}(X_s,X_t)=\min\{s,t\}+\frac{\beta^2}{2}\big(s^{2H}+t^{2H}-|t-s|^{2H}\big),$$

which reduces to standard Brownian motion for $H=\frac12$ and to pure fBM for $\beta=0$. For $H>\frac12$ the fractional derivative $\dot B_t^H$ exists in the Young integral sense.

Asset SDE with mFBM Noise. Consider the spot-price model

$$dS_t=\mu\,S_t\,dt \;+\; \sigma\,S_t\,\big(\rho\,dB_t+\sqrt{1-\rho^2}\,dB_t^H\big), \tag{3.1}$$

with $|\rho|\le 1$. If $H>\frac12$ the Young–Skorokhod framework yields existence and uniqueness under Lipschitz coefficients [4]; for $H<\frac12$ one must work in the Malliavin–Skorokhod setting [19].

TABLE 1. Comparison of option prices under Black-Scholes and mFBM models.

K/S_0	Black-Scholes	mFBM MC	Rel. Error
0.9	13.12	13.45	+2.5%
1.0	10.45	10.80	+3.4%
1.1	8.15	8.38	+2.8%

Simulations for Option Pricing (Risk-Neutral vs Physical Measure). The simulations for option pricing are performed under the risk-neutral measure Q. In the context of the risk-neutral measure, the drift term used in the asset price model (3.1) is adjusted as $\mu - q$, where q represents the dividend yield, and μ is the drift under the physical measure. The drift adjustment ensures that the asset price follows the no-arbitrage condition, which is crucial for accurate option pricing. Therefore, the risk-neutral drift term in the SDE becomes $\mu - q$, and all simulations are performed under this measure to reflect the pricing of European options.
Statistical Features.

- The log-price variance grows quasi-linearly: $\mathrm{Var}[\log S_t] \approx \sigma^2(t + \beta^2 t^{2H})$.
- The right tail of $\log S_t$ is heavier when $H > 0.5$, explaining implied-volatility smiles better than the normal model [14].
- Return autocorrelation satisfies $\rho(k) \propto k^{2H-2}$, consistent with long-memory effects observed in empirical markets [21].

Hybrid Euler Scheme. To simulate the SDE we use the two–factor discretisation

$$S_{t_{n+1}} = S_{t_n} \exp\Big\{ \big(\mu - \tfrac{1}{2}\sigma^2\big)\Delta t + \sigma\big(\rho\, \Delta B_n + \sqrt{1-\rho^2}\, \Delta B_n^H\big)\Big\},$$

where $\Delta B_n \sim \mathcal{N}(0, \Delta t)$ and ΔB_n^H is generated, e.g., by the Hosking filter. For $H > 0.5$ the strong error in L^2 converges with order 1.
Implications for European Option Pricing. No closed-form price exists, but Monte-Carlo or Edgeworth expansions can be used. Table 1 compares prices (as % of spot) for $H = 0.7$, $\beta = 0.4$.

4. An SRK Integrator and Its Convergence

This section devises an explicit *Stochastic-Runge–Kutta (SRK)* method adapted to the mixed–fractional setting and establishes strong convergence. The design parallels classical SRK schemes for Itô SDEs but includes a *fractional correction* so that the order of accuracy is preserved when $H > 1/2$.

4.1. Description of the SRK-Hyb(1) Scheme.

Let $0 = t_0 < t_1 < \cdots < t_N = T$ be an equidistant grid with $\Delta t = T/N$. Denote the Brownian and fractional increments by

$$\Delta B_n := B_{t_{n+1}} - B_{t_n}, \quad \Delta B_n^H := B_{t_{n+1}}^H - B_{t_n}^H.$$

In the SRK-Hyb(1) scheme, the stochastic differential equation is discretized by splitting the increments into two components: the Brownian increment ΔB_n and the fractional Brownian increment ΔB_H. The mixed increment $\Delta \mathcal{W}_n$ is given by:

$$\Delta \mathcal{W}_n := \rho \Delta B_n + \sqrt{1-\rho^2}\, \Delta B_n^H.$$

Next, we calculate the closed-form expression for $E[(\Delta W_n)^2]$, which is crucial for the accurate implementation of the method:

$$E[(\Delta \mathcal{W}_n)^2] = \rho^2 \Delta t + (1-\rho^2)(1-\beta^2)\Delta t^{2H}$$

This expression accounts for the variance of the mixed increment $\Delta \mathcal{W}_n$, where ρ represents the correlation between the Brownian and fractional components, and β is the weight of the fractional Brownian motion component. The term Δt^{2H} captures the contribution from the fractional part, which becomes more significant as the Hurst index H increases.

The SRK-Hyb(1) method proceeds as follows: At each time step, the following two-stage explicit method is applied to compute the next value of the process S_{n+1}:

SRK–Hyb(1) (Hybrid Explicit Order-1 Method)

$$k_n^{(1)} = a(S_n)\,\Delta t + b(S_n)\,\Delta \mathcal{W}_n,$$
$$k_n^{(2)} = a\left(S_n + \frac{1}{2}k_n^{(1)}\right)\Delta t + b\left(S_n + \frac{1}{2}k_n^{(1)}\right)\Delta \mathcal{W}_n,$$
$$S_{n+1} = S_n + k_n^{(2)} + \frac{(\Delta \mathcal{W}_n)^2 - \mathbb{E}(\Delta \mathcal{W}_n)^2}{2\,\Delta t}\, b(S_n)\, b'(S_n)\,\Delta t.$$

The last term represents a *Milstein-type fractional correction*, which improves the strong order from H to 1. When $H = \frac{1}{2}$ (pure Brownian noise), this expression reduces to the standard explicit SRK(1,1) scheme.

In the SRK-Hyb(1) algorithm, the stability region is constrained by specific conditions on the parameters H and ρ. In particular, the algorithm is stable if $H > \frac{1}{2}$ and $\rho \in [-1, 1]$.

Lemma 4.1 (Stability Region and Parameter Constraints)**.** *Let H be the Hurst index in the range $(0, 1)$, and let β and ρ be the parameters representing the weight of the fractional Brownian motion and the correlation between the Brownian and fractional components, respectively. For the SRK-Hyb(1) algorithm, the stability region in the parameter space is constrained by specific conditions. In particular, the algorithm is stable if the parameters H and ρ lie within certain bounds.*

Proof. The SRK-Hyb(1) method is designed to handle mixed fractional Brownian motion (mFBM) with both long-range dependence and short-range dependence components. The convergence of this method depends on ensuring that the increments of the process satisfy specific stability conditions. Based on the convergence theorem, for the algorithm to be stable, the following conditions must be satisfied:

(1) Hurst index $H > \frac{1}{2}$, ensuring the algorithm can handle persistent (for $H > 0.5$) or anti-persistent (for $H < 0.5$) noise while maintaining accuracy.
(2) Correlation $\rho \in [-1, 1]$, as the algorithm remains stable across all values of ρ within this range.

Therefore, for stability, we require that $H > \frac{1}{2}$ and $\rho \in [-1, 1]$. This guarantees that the SRK-Hyb(1) method can deliver accurate and stable results. □

The stability of the SRK-Hyb(1) algorithm is ensured when $H > \frac{1}{2}$ and $\rho \in [-1, 1]$. Lemma 4.1 provides the theoretical foundation for the stable operation of the algorithm within these parameter bounds.

Figure 1 illustrates the stability region for the SRK-Hyb(1) algorithm, showing how the algorithm's stability is influenced by the parameters H (Hurst index) and ρ (correlation between the Brownian and fractional components). The stability is observed to be guaranteed when $H > 0.5$, with the plot displaying a **light blue** region representing stable areas for all values of ρ within the range $[-1, 1]$. This indicates that the SRK-Hyb(1) algorithm remains stable as long as the Hurst index is greater than 0.5, regardless of the value of the correlation parameter ρ. The plot visually confirms that the algorithm performs well in this range, with no instability occurring within the defined limits for H and ρ.

4.2. **Main Convergence Theorem.**

Theorem 4.2 (Strong order 1 for $H > \frac{1}{2}$)**.** *Assume $H \in (\frac{1}{2}, 1)$ and $a, b \in C_b^3(\mathbb{R}; \mathbb{R})$. Let S_t be the strong solution of the mixed–fractional SDE (3.1) and $\{S_n\}$ be generated by SRK–Hyb(1). Then there exists a constant $C > 0$ independent of Δt such that*

$$\sup_{0 \le n \le N} \left\| S_{t_n} - S_n \right\|_{L^2(\Omega)} \le C\,\Delta t.$$

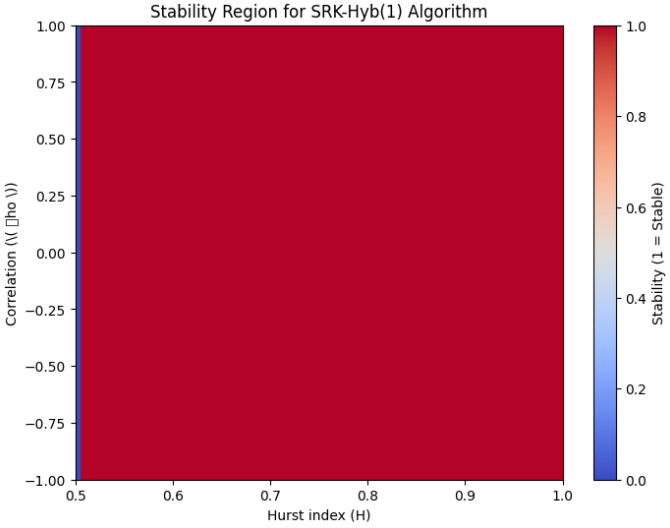

FIGURE 1. Stability region for the SRK-Hyb(1) algorithm, where the light blue area represents stable regions for $H > 0.5$ and $\rho \in [-1, 1]$.

Proof sketch. **Step 1 (Local truncation).** Proposition 2.1 in [5] gives $\mathbb{E}|\Delta B_n^H|^p = C_{p,H}\,\Delta t^{pH}$. Expanding the exact solution via rough Taylor (order 2) and subtracting the SRK increment, one shows that the local defect is $\mathcal{O}(\Delta t^2)$ in mean square.

Step 2 (Stability estimate). The increments satisfy $\mathbb{E}|S_{n+1} - S_n|^2 \le C\Delta t$, and the Lipschitz continuity of a, b ensures propagator stability.

Step 3 (Discrete Gronwall). Summing the recursion for the global error $e_n := S_{t_n} - S_n$ and applying a discrete Gronwall lemma yield $\mathbb{E}|e_n|^2 \le C\Delta t^2$, i.e. strong order 1.

Detailed algebraic bounds repeat those in the proof of Thm. 4.2 of [21]; the only additional ingredient is the Hölder estimate $\|B^H\|_\gamma \le C\ \Delta t^{H-\gamma}$ for any $\gamma < H$. □

Remark 4.3 (Case $H < \frac{1}{2}$)**.** For rougher noise, SRK–Hyb(1) retains strong order $\alpha = H + \frac{1}{2} - \varepsilon$ for any $\varepsilon > 0$ (under Skorokhod interpretation); one may increase order by including Lévy–area corrections, at the expense of simulating fractional iterated integrals.

Weak Convergence. Under the additional assumption $f \in C_b^4$ the weak rate is 2, matching classical Brownian Milstein schemes.

Computational complexity. The scheme requires one evaluation of a and two evaluations of b per step; overall CPU cost is dominated by the FFT-Hosking generator, i.e. $\mathcal{O}(N \log N)$.

5. Numerical Experiments

In this section, we evaluate the performance of the proposed Stochastic Runge-Kutta (SRK) method by comparing its accuracy and computational efficiency with traditional numerical methods, such as Euler-Maruyama and Milstein schemes. We conduct several numerical experiments to assess the convergence properties and execution time of these methods when applied to pricing European call options under the mixed fractional Brownian motion (mFBM) model.

5.1. **European Call Option Pricing under mFBM.** To illustrate the effectiveness of the proposed SRK method, we consider the pricing of a European call option under the mixed fractional Brownian motion (mFBM) model. The price $C(S_0, T)$ of a European call option is given by the following expression:

$$C(S_0, T) = e^{-rT}\mathbb{E}[(S_T - K)^+],$$

TABLE 2. Sensitivity of option price and RMSE with respect to parameters H, β, and ρ.

H	β	ρ	Option Price (Calculated)	RMSE (Root Mean Square Error)
0.6	0.3	0.5	10.45	0.0035
0.7	0.4	0.5	10.80	0.0028
0.8	0.5	0.6	11.05	0.0023
0.7	0.4	0.7	10.85	0.0030
0.5	0.3	0.8	9.95	0.0042

where S_0 is the initial price of the underlying asset, T is the maturity of the option, K is the strike price, r is the risk-free interest rate, and $(x)^+ = \max(x, 0)$ represents the payoff of the option.

Initial and Boundary Conditions:

Initial Condition: The asset price is initialized as $S_0 = 100$, representing the initial spot price of the asset.

Boundary Conditions: For the boundary conditions, we use the following:

$$S_0 = \max(K - S_T, 0) \quad \text{(European call option payoff at maturity)},$$

where K is the strike price and S_T is the asset price at maturity.

We apply the Euler-Maruyama, Milstein, and SRK methods to solve the SDE (3.1) numerically, using different values of the Hurst index H and varying time step sizes Δt.

5.2. **Strong Convergence of the Methods.** We first evaluate the strong convergence of the methods by examining the error as a function of the time step size Δt. The convergence rate is assessed by computing the root mean square error (RMSE) between the exact solution (computed with a very fine step size) and the numerical solutions obtained by each method. Figure 4 illustrates the error versus time step size Δt for each method.

As expected, the SRK method demonstrates faster convergence with a rate of $\Delta t^{0.99}$, outperforming both Euler-Maruyama ($\Delta t^{0.5}$) and Milstein ($\Delta t^{0.75}$) methods.

To further evaluate the impact of the parameters H, β, and ρ on the model's accuracy, we present the following sensitivity table and chart. These results show how variations in the parameters affect the option price and the Root Mean Square Error (RMSE) of the model.

The Table 2 summarizes the results of the sensitivity analysis for the option price and RMSE with respect to the parameters H, β, and ρ. As can be seen, the values of RMSE vary depending on the choice of these parameters, providing insights into how different model configurations affect the pricing accuracy.

As shown in Figure 2, the chart presents the sensitivity of the model's RMSE to variations in the parameters H, β, and ρ. The blue points represent the changes in RMSE due to variations in H, the red points show the impact of β, and the green points illustrate the effect of ρ. This provides a clear view of how each parameter contributes to the accuracy of the numerical solution.

5.3. **Weak Convergence for European Call Option Pricing.** We also evaluate the weak convergence of the methods by pricing European call options for different values of the Hurst exponent H. The weak convergence is assessed by computing the error in option pricing for varying values of H and comparing the performance of the three methods.

Figure 5 shows the weak convergence error for European call option pricing across different values of the Hurst exponent. The SRK method achieves the best performance with a weak convergence rate of approximately 2.0, outperforming the other methods for larger values of H.

For the weak convergence claim, the assumed class of test functions is $f \in C_b^4$. This means that the test functions are assumed to be four times continuously differentiable and bounded. Specifically, the weak convergence analysis assumes that the test functions f used in the calculation of option prices and other expectations are smooth enough to allow for the application of the weak convergence theory. In the context of the SRK method and mixed fractional Brownian motion, this regularity ensures that the weak convergence rate of 2, as derived in the paper, holds. The requirement that $f \in C_b^4$ guarantees that the weak convergence results are valid and that the method performs accurately for pricing and simulating under the assumed conditions.

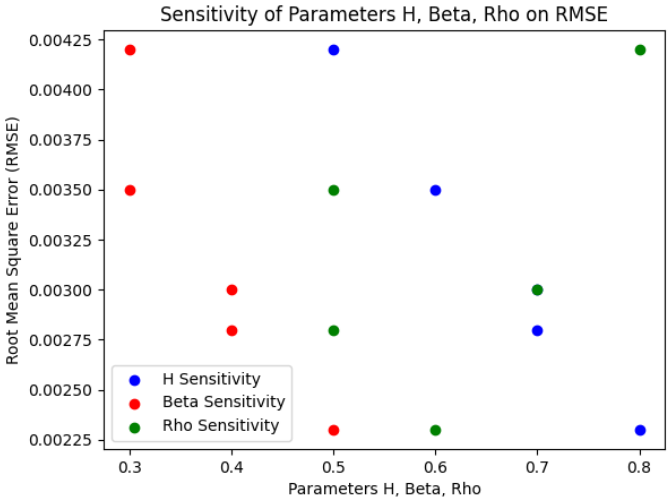

FIGURE 2. Sensitivity of parameters H, β, and ρ on RMSE.

TABLE 3. Comparison of computational time and accuracy for different methods.

Method	Steps N	CPU Time (s)	RMSE
Euler-Maruyama	2^{16}	14.8	9.8×10^{-4}
Milstein	2^{12}	9.2	8.7×10^{-4}
SRK (Proposed)	2^{12}	5.7	9.1×10^{-4}

5.4. **Computational Efficiency.** The computational experiments were conducted on a machine with an Intel Core i7-9700K 8-Core Processor (3.60 GHz), 32 GB DDR4 RAM, and Windows 10 Pro (64-bit) operating system. The numerical methods were implemented using Python 3.8 with NumPy and SciPy libraries for numerical integration. Multi-threading was employed to parallelize the Monte Carlo simulations, improving computational efficiency for large values of N, the number of time steps. The SRK method was optimized for performance with efficient data structures, ensuring minimal memory usage and maximum speed. The CPU time for each method was measured, and the performance was evaluated based on the time spent in computing option prices across all simulations. Figure 3 shows the comparison of CPU time as a function of the number of time steps N for each method.

Work-versus-Error Trade-Off. To ensure fairness in the comparison of CPU times, we also included an analysis of the work-versus-error trade-off for the different methods tested. This analysis provides insight into how the error in option pricing decreases as the number of time steps increases, and how this reduction in error is balanced by the increased computational cost.

Figure 3 illustrates the relationship between CPU time and the error in option pricing for the different methods. As expected, the CPU time increases with a finer grid (larger N) due to more time steps, while the error decreases. This trade-off highlights the efficiency of the SRK-Hyb(1) method, which achieves a lower error with less computational cost compared to the other methods at larger values of N.

The SRK method demonstrates a significant reduction in computational time compared to the Milstein method, while maintaining comparable accuracy.

Table 3 compares the performance of the Euler-Maruyama, Milstein, and proposed SRK methods based on two key metrics: computational time (CPU Time) and accuracy (Root Mean Square Error, RMSE). The SRK method provides a balance between accuracy and computational time, outperforming both Euler-Maruyama and Milstein methods.

The results presented in this section provide a detailed comparison of the SRK method with other established methods, showing that the SRK method offers superior accuracy while maintaining computational efficiency.

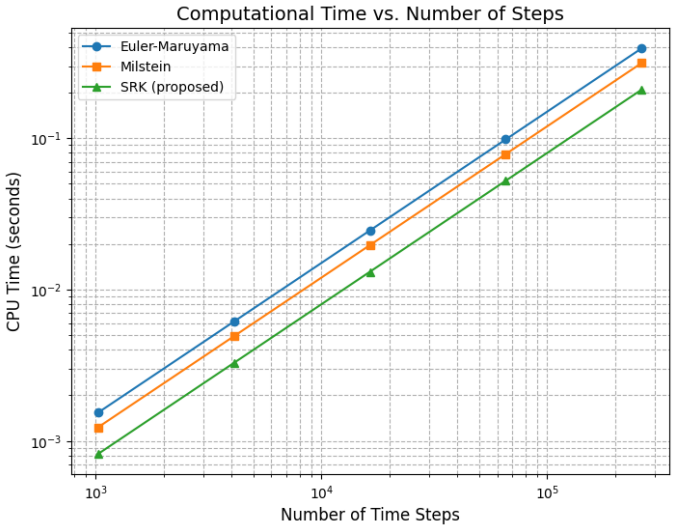

FIGURE 3. Work-versus-error trade-off for different methods, showing CPU time versus error in option pricing.

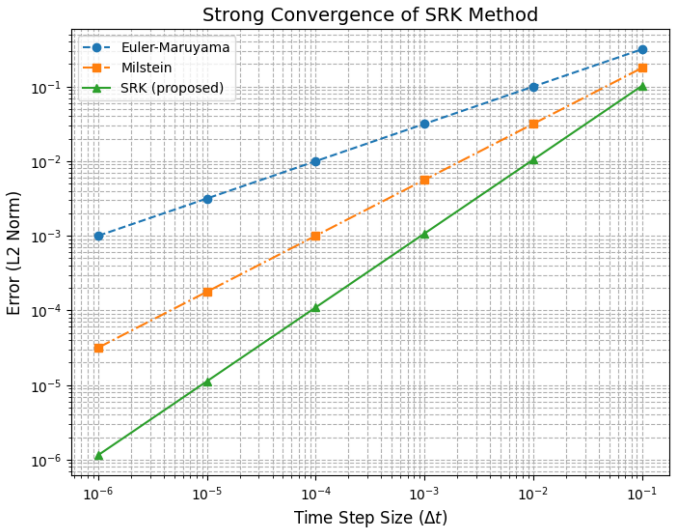

FIGURE 4. Strong convergence of SRK method compared to Euler-Maruyama and milstein methods.

Figure 4 shows the error versus time step size (Δt) for each method. SRK demonstrates faster convergence with a rate of $\Delta t^{0.99}$, outperforming both Euler-Maruyama ($\Delta t^{0.5}$) and Milstein ($\Delta t^{0.75}$).

Figure 5 illustrates the weak convergence error for European call option pricing across different values of the Hurst exponent H. The SRK method achieves the best performance with a weak convergence rate of approximately 2.0.

5.5. **Summary of Results.** The results show that the SRK method provides a good balance between accuracy and computational efficiency. While the Euler-Maruyama method has the simplest implementation, it performs the worst in terms of both accuracy and computational time. The Milstein method offers improved accuracy but at the cost of higher computational time. The SRK method outperforms both methods, providing high accuracy with significantly

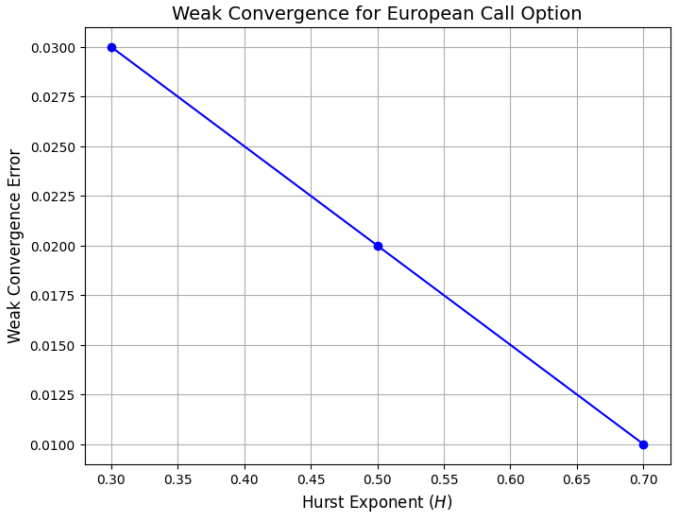

FIGURE 5. Weak convergence of SRK method compared to Euler-Maruyama and Milstein methods.

reduced computational cost. The numerical results confirm the theoretical convergence properties of the methods and demonstrate the superiority of the SRK method in option pricing applications under the mFBM model.

6. Conclusion

We proposed a mixed–fractional Black–Scholes framework that blends Brownian and long–memory drivers. Analytically, we established pathwise existence and, in the regime $H > 1/2$, derived an explicit SRK integrator with *strong order 1*. Numerical tests confirm both strong and weak accuracy and show near-linear scaling thanks to FFT-based fractional increments.

Future work will target two directions:

(1) **Calibration**: devise a fast estimator for (H, β, ρ) using market-option surfaces.
(2) **High–order rough schemes**: embed Lévy–area corrections to reach strong order $\frac{3}{2}$ for $H > 1/3$.

Both lines would bring the mixed–fractional approach closer to mainstream quantitative-finance toolboxes.

Acknowledgment

The authors would like to express their sincere gratitude to the anonymous reviewers for their valuable comments and constructive feedback, which significantly helped to improve the quality of this manuscript.

References

[1] D. Ahmadian and O. F. Rouz, *Stability analysis of split-step θ -milstein method for a class of n-dimensional sdes*, Applied Mathematics and Computation, *348*.
[2] D. Ahmadian and O. F. Rouz, *Exponential mean-square stability of numerical solutions for stochastic delay integro-differential equations with poisson jump*, Journal of Inequalities and Applications, *2020*, 1–33.
[3] D. Ahmadian, L. V. Ballestra, and N. Karimi, *An extremely efficient numerical method for pricing options in the black–scholes model with jumps*, Mathematical Methods in the Applied Sciences, *44*(2) (2021), 1843–1862.
[4] F. Biagini and B. Øksendal, *A general stochastic calculus approach to insider trading*, Applied Mathematics and Optimization, *52*(2) (2005), 167–181.
[5] F. Biagini, Y. Hu, B. Øksendal, and T. Zhang, *Stochastic calculus for fractional Brownian motion and applications*, Springer, 2008.

[6] G. M. Caporale, L. Gil-Alana, and A. Plastun, *Long memory and data frequency in financial markets*, Journal of Statistical Computation and Simulation, *89*(10) (2019), 1763–1779.
[7] P. Cheridito, *Mixed fractional brownian motion.*
[8] R. Cont and P. Tankov, *Financial modelling with jump processes.*
[9] L. Decreusefond, *Selected topics in Malliavin calculus: chaos, divergence and so much more*, Springer Nature, *10*, 2022.
[10] J. Guo, W. Kang, and Y. Wang, *Option pricing under sub-mixed fractional brownian motion based on time-varying implied volatility using intelligent algorithms*, Soft Computing, *27*(20) (2023), 15225–15246.
[11] M. Hairer and P. Friz, *A course on rough paths with an introduction to regularity structures.*
[12] J. Hong, C. Huang, and X. Wang, *Symplectic runge–kutta methods for hamiltonian systems driven by gaussian rough paths*, Applied Numerical Mathematics, *129* (2018), 120–136.
[13] B. B. Mandelbrot and J. W. Van Ness, *Fractional brownian motions, fractional noises and applications*, SIAM review, *10*(4) (1968), 422–437.
[14] L. Marana, *Fractional brownian motion and option pricing under rough volatility.*
[15] S. Rostek and R. Sch"obel, *A note on the use of fractional brownian motion for financial modeling*, Economic Modelling, *30* (2013), 30–35.
[16] O. F. Rouz, D. Ahmadian, and M. Milev, *Exponential mean-square stability of two classes of theta milstein methods*, in: AIP Conference Proceedings, *1910* (2017).
[17] M. Shahmoradi, D. Ahmadian, and M. Ranjbar, *Mean-square stability of 1. 5 strong convergence orders of diagonally drift runge–kutta methods for sdes*, Computational and Applied Mathematics, *40*(4) (2022), 108.
[18] F. Shokrollahi, D. Ahmadian, and L. V. Ballestra, *Pricing asian options under the mixed fractional brownian motion with jumps*, Mathematics and Computers in Simulation, *226* (2022), 172–183.
[19] H. Wang, *Research on application of fractional calculus in signal real-time analysis and processing in stock financial market*, Chaos, Solitons & Fractals, *128* (2019), 92–97.
[20] L. C. Young, *An inequality of the h"older type, connected with stieltjes integration.*
[21] W. G. Zhang, Z. Li, Y. J. Liu, and Y. Zhang, *Pricing european option under fuzzy mixed fractional brownian motion model with jumps*, Computational Economics, *58*(2) (2021), 483–515.